Gap solitons in Ginzburg-Landau media

Hidetsugu Sakaguchi[1] and Boris A. Malomed[2]
[1]*Department of Applied Science for Electronics and Materials, Interdisciplinary Graduate School of Engineering Sciences, Kyushu University, Kasuga, Fukuoka 816-8580, Japan*
[2]*Department of Physical Electronics, School of Electrical Engineering, Faculty of Engineering, Tel Aviv University, Tel Aviv 69978, Israel*
(Received 2 March 2008; published 19 May 2008)

We introduce a model combining basic elements of conservative systems which give rise to gap solitons, i.e., a periodic potential and self-defocusing cubic nonlinearity, and dissipative terms corresponding to the complex Ginzburg-Landau (CGL) equation of the cubic-quintic type. The model may be realized in optical cavities with a periodic transverse modulation of the refractive index, self-defocusing nonlinearity, linear gain, and saturable absorption. By means of systematic simulations and analytical approximations, we find three species of stable *dissipative gap solitons* (DGSs), and also dark solitons. They are located in the first finite band gap, very close to the border of the Bloch band separating the finite and the semi-infinite gaps. Two species represent loosely and tightly bound solitons, in cases when the underlying Bloch band is, respectively, relatively broad or very narrow. These two families of stationary solitons are separated by a region of breathers. The loosely bound DGSs are accurately described by means of two approximations, which rely on the product of a carrier Bloch function and a slowly varying envelope, or reduce the model to *CGL-Bragg equations*. The former approximation also applies to dark solitons. Another method, based on the variational approximation, accurately describes tightly bound solitons. The loosely bound DGSs, as well as dark solitons, are mobile, and their collisions are quasielastic.

DOI: 10.1103/PhysRevE.77.056606 PACS number(s): 05.45.Yv, 03.75.Lm, 42.65.Tg

I. INTRODUCTION AND THE MODEL

Complex Ginzburg-Landau (CGL) equations are well known as basic models for pattern formation in various nonlinear dissipative media [1]. In addition to that, they find direct realizations in nonlinear optics, hydrodynamics, chemical waves, and other areas [2]. An important class of objects predicted by the CGL equations are solitary pulses, alias "dissipative solitons." They may represent, in particular, pulses of traveling-wave convection in channels [3] and optical signals generated by fiber lasers, the latter area being very important for applications [4,5].

The simplest CGL equation is one with the cubic nonlinearity. Exact solutions for pulses are available in that case [6], but they are unstable. A modified equation that can support stable pulses includes the cubic-quintic (CQ) nonlinearity, i.e., a combination of linear loss, cubic gain, and quintic loss, the latter term securing the overall stability of the model. The CGL equation of the CQ type was first proposed (in the two-dimensional form) by Petviashvili and Sergeev [7]. In the one-dimensional version of the CQ-CGL equation, stable solitary-pulse solutions were predicted by means of an analytical approximation, which treated them as a modification of solitons of the nonlinear Schrödinger equation [8]. Later, they were studied in detail, chiefly by means of numerical simulations [9,10]. More general models, such as the complex Swift-Hohenberg equation with the CQ nonlinearity [11], and systems of linearly coupled CQ-CGL equations [12], were developed too.

Besides the classical solitons of the nonlinear-Schrödinger type, another generic species of solitary waves in conservative media are gap solitons (GSs). They are important objects both in nonlinear optics (represented, first of all, by temporal solitons in fiber Bragg gratings) and in Bose-Einstein condensates (BECs) with repulsive interactions between atoms, which are trapped in optical-lattice potentials. A characteristic feature, which had given the gap solitons their name, is the fact that their wave number (in terms of optics) falls into a finite band gap induced by the effective periodic potential acting in the medium. In the context of both fiber gratings [13–15] and BEC [16,17], gap solitons were predicted theoretically, including two-dimensional matter waves of the gap-soliton type [18,19]. Following these predictions, the creation of optical and matter-wave gap solitons in effectively one-dimensional settings was reported, respectively, in short segments of fiber gratings [20], and in the condensate of ^{87}Rb atoms loaded into an optical lattice [21].

A new physical setting may be expected as a result of the interplay between the periodic-potential background, which is responsible for the existence of GSs in conservative nonlinear media, and the CQ dissipative nonlinearity which stabilizes the ordinary dissipative solitons in media modeled by CGL equations. The basic equation of the CGL type, which incorporates these ingredients, takes a relatively simple form (if proper rescalings were used to minimize the number of free parameters) as follows:

$$i\frac{\partial \phi}{\partial t} = -\frac{1}{2}\frac{\partial^2 \phi}{\partial x^2} + [|\phi|^2 - \varepsilon \cos(\pi q x)]\phi + i(-\gamma_1 + \gamma_3|\phi|^2 - \gamma_5|\phi|^4)\phi, \quad (1)$$

where ϕ is the local amplitude of the electromagnetic wave (in terms of the optical model), ε and $2/q$ are the amplitude and period of the lattice potential, and positive coefficients γ_1, γ_5, and γ_3 account for, respectively, the linear and quintic dissipation and cubic gain in the CQ-CGL model. The self-

defocusing nonlinearity, which appears in Eq. (1), is most relevant to GSs; in the case of self-attraction, GSs are less significant objects, as it is then much easier to create ordinary solitons with the wave number belonging to the semi-infinite gap. A quintic self-defocusing term is not included in Eq. (1), as, in optical media, it always represents a small correction to its cubic counterpart (it may be more important when it represents a higher-order nonlinearity competing with the cubic self-focusing, in the presence of a periodic potential [22]).

A direct physical realization of Eq. (1) is provided by a planar optical waveguide, with the self-defocusing cubic nonlinearity, in which the lattice potential accounts for a periodic transverse modulation of the refractive index, while the CQ dissipative terms represent (as usual), a combination of the linear amplification and saturable absorption. The latter ingredient is common to laser cavities (such as fiber lasers [5,23]). In terms of the planar waveguide, variable t in Eq. (1) is actually the propagation distance, x is the transverse coordinate, and the second derivative accounts for diffraction in the paraxial approximation. Note that Eq. (1) does not include a diffusion (alias viscosity) term, $\sim i\phi_{xx}$: while it is a usual ingredient of more general models of the CGL type [1], this term does not have a straightforward meaning in the equation for the spatial evolution of optical beams. In fact, the absence of the viscosity allows dynamical effects, which would be suppressed otherwise, such as the creation of moving solitons (*tilted beams*, in terms of spatial optics) and collisions between them [10].

Thus, the proposed setup should make it possible to create optical gap solitons (in the spatial domain), supported by the balance between the cubic gain and linear and quintic dissipation. We call these states *dissipative gap solitons* (DGSs). Besides the general interest, this new species of dissipative solitons offers potential applications. Indeed, the sensitivity of the results to the normalized gain strength, γ_3/γ_1, along with the ease of the creation of tilted ("moving") solitons and controllable character of collisions between them (see below), suggest that the present setting may be used to realize soliton switching and other all-optical operations.

The paper is organized as follows. In Sec. II, we start by identifying the location of DGS families with respect to the underlying band-gap spectrum. It is concluded that all solitons are found in the first finite band gap, very close to the border of the Bloch band, which separates the band gap from the semi-infinite one. Further, two distinct soliton species are identified, namely, loosely and tightly bound ones (i.e., broad and narrow solitons). The former family is separated from the semi-infinite gap by a relatively broad Bloch band, while the latter one sits on top of a very narrow band. The two families of the stationary solitons are separated by a region of breathers. We develop two analytical approximations for the loosely bound DGSs. One of them, elaborated in Sec. II, represents the soliton as a product of an underlying Bloch function and a slowly varying envelope (this approximation turns out to be very accurate for both bright and dark solitons). The other approach, presented in Sec. III, reduces Eq. (1) to coupled-mode equations, i.e., a system of *CGL-Bragg equations*. In Secs. II and III, we also demonstrate that loosely bound dissipative solitons, both bright and dark ones, can be readily set in motion, and collisions between bright solitons are quasielastic, leading to an increase of their velocities. Tightly bound solitons are considered in Sec. IV, where an accurate analytical description for them is developed on the basis of the variational approximation. The paper concludes with Sec. V.

II. LOOSELY BOUND SOLITONS

A. General structure of soliton families

Families of stable dissipative solitons can be found from direct simulations of Eq. (1), as they are *attractors* of this equation. The simulations were performed by means of the split-step method, typically in the x domain of width $L=50$ or 100. Generic families of the dissipative soliton states can be represented by a set of stable localized solutions generated for the following set of parameters:

$$\varepsilon = 5, \quad \gamma_1 = 0.01, \quad \gamma_3 = 0.2, \quad \gamma_5 = 0.6, \tag{2}$$

while the lattice wave number q is varied (the variation of q makes it possible to test the "gap-soliton" nature of the solutions). The small value of linear-loss coefficient γ_1 in set (2) is sufficient to secure the stability of the solitons against perturbations of the background around them. As concerns the DGSs, it will be seen below that a typical value of their amplitude is $\simeq 0.5$ [see Figs. 2(b), 4, 5(b), and 8(a)]. Estimating average values of $|\phi(x)|^2$ and $|\phi(x)|^4$ as per these figures, one can conclude that the values of the coefficients in set (2) corresponds to, roughly, equal effective strengths (dissipation rates) induced by the linear and quintic loss terms, which together compensate the gain provided by the cubic term. In experimental setups (laser cavities), the effective values of the loss and gain coefficients can be easily adjusted in broad limits [4]. Comparison with cavity models incorporating saturable absorbers demonstrates that the typical values of the scaled coefficients fixed in Eq. (2) are quite realistic.

Stationary solutions to Eq. (1) are sought for as $\phi = e^{-i\mu t}u(x)$, where $u(x) \equiv |\phi(x)|$ is a real localized function. The squared width of the soliton is defined (numerically) as $w^2 = \int (x-x_0)^2 |\phi(x)|^2 dx / \int |\phi(x)|^2 dx$, where x_0 is the central point of the localized state, and the integration is performed over the entire spatial domain. Characteristics of the soliton families, obtained by varying q while other parameters are fixed as per Eq. (2), i.e., dependences $w(q)$ and $\mu(q)$, are displayed in Fig. 1.

A fundamentally important feature of the soliton family is its location with respect to the band-gap structure defined by the linearized version of Eq. (1), with $\gamma_1 = 0$, i.e., the Mathieu equation [see Eq. (4) below]. The conclusion which is evident in Fig. 1(b) is that the entire family belongs to the first finite band gap, running near its lower edge; i.e., very close to the border of the first Bloch band which separates the finite band gap from the semi-infinite one. The same conclusion is true for families of dissipative solitons found at other values of ε and $\gamma_{1,3,5}$.

Figure 1(a) shows a clear trend to an increase of the soliton's width with q (particular examples of both broad and narrow solitons are displayed below). An irregularity in the

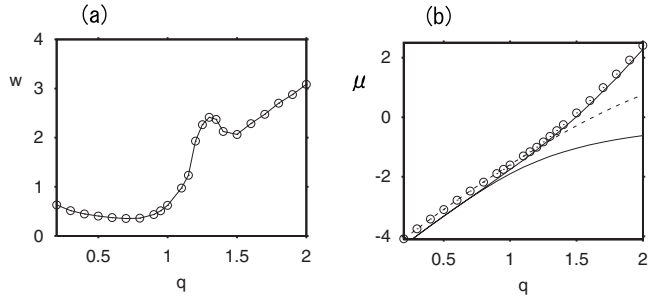

FIG. 1. Chains of circles in panels (a) and (b) display width w and frequency μ of the numerically found dissipative solitons as functions of wave number q of the periodic potential, while the other parameters are fixed as per Eq. (2). The continuous curve in panel (a) is a guide to the eye (chains of circles represent numerically found data in other figures too). In panel (b), two solid curves show the edges of the first Bloch band calculated from the linearized (Mathieu) equation for $\varepsilon=5$ and $\gamma_1=0$ (see the text), while the dashed line is the $\mu(q)$ dependence as predicted by the analytical approximation for narrow (tightly bounds) solitons [see Eqs. (29) and (30)].

$w(q)$ dependence around $q=1.3$ is explained by the fact that the numerically found localized solutions are *breathers*, rather than stationary states, in the interval of $1.15<q<1.46$, which separates tightly bound (narrow) and loosely bound (broad) solitons, as shown in detail in Fig. 2 (Fig. 1 shows time-average values of the width and frequency for the breathers).

The amplitude of the intrinsic oscillations of the breather, which is presented as a function of q, in Fig. 2(c), is defined as $(\Delta A)^2=\langle[A(t)-\langle A(t)\rangle]^2\rangle$, where $A(t)$ is the largest value of $|\phi(x,t)|$ for given t, and $\langle\ldots\rangle$ stands for the time averaging. Naturally, ΔA vanishes at the edges of the interval where the breathers exist. Note that the oscillation amplitude is always small.

B. Description of loosely bound solitons in terms of Bloch functions

1. General analysis

Here we aim to develop a systematic analysis of the DGSs found at larger values of q, when the first finite band gap, where they are located in Fig. 1(b), is separated from the semi-infinite gap by a relatively broad Bloch band. In this case, the proximity of the solitons to the upper edge of the Bloch band suggests using the following ansatz [17,18]:

$$\phi(x,t)=e^{-i\mu_0 t}F(x)\Phi(x,t), \tag{3}$$

where $F(x)$ is a Bloch function, which is to be found as a solution to the Mathieu equation,

$$\mu_0 F(x)=(1/2)F''+\varepsilon\cos(\pi q x)F \tag{4}$$

(a relation between μ_0 and the actual soliton frequency μ is given below). As usual, the quasiperiodic Bloch function may be represented as $F(x)=e^{ikx}f(x)$, where k is the quasimomentum, and function $f(x)$ is periodic, $f(x+2/q)=f(x)$. Typical results for DGSs are reported here for $q=2$, i.e., when the period of the lattice potential is 1. Then, the solution to the Mathieu equation determines the corresponding band structure, $\mu_0=\mu_0(k)$, points $k=0$ and $k=\pi$ being, respectively, the center and edge of the first Brillouin zone (BZ).

For small-amplitude solutions, $\Phi(x,t)$ in Eq. (3) is a slowly varying envelope function. Substituting this ansatz in Eq. (1) and performing the averaging as per Ref. [18], one can derive an equation of the slow evolution for the envelope, which is tantamount to the CQ-CGL equation with constant coefficients, as follows:

$$i\frac{\partial\Phi}{\partial t}=-\frac{1}{2}m_{\text{eff}}^{-1}\frac{\partial^2\Phi}{\partial x^2}+g_3|\Phi|^2\Phi + i(-\gamma_1+g_3\gamma_3|\Phi|^2-g_5\gamma_5|\Phi|^4)\Phi, \tag{5}$$

where effective mass m_{eff} for linear excitations and average nonlinear coefficients are

$$m_{\text{eff}}^{-1}=\mu_0''(k),\quad g_n=\int_0^1|F(x)|^{n+1}dx/\int_0^1|F(x)|^2dx,\quad n=3,5. \tag{6}$$

In the case of $m_{\text{eff}}<0$ and $\gamma_1=\gamma_3=\gamma_5=0$, Eq. (5) has an obvious bright-soliton solution,

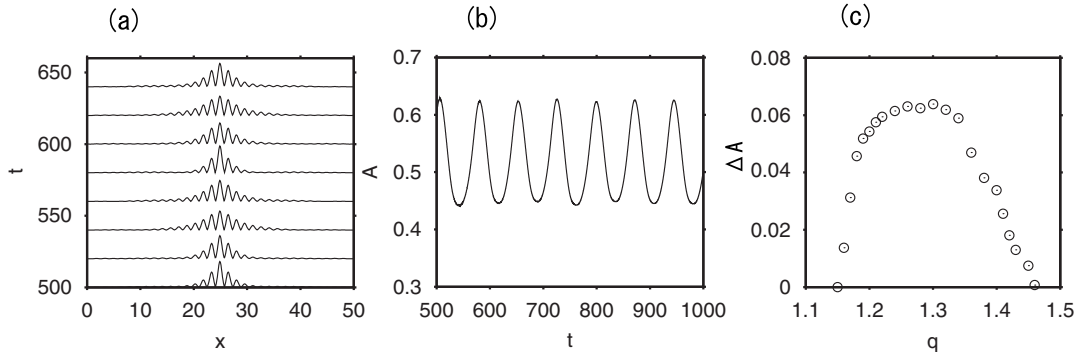

FIG. 2. (a) A set of snapshots illustrating the periodic evolution of the breather at $q=1.3$. (b) The amplitude of this breather as a function of t. (c) The amplitude of intrinsic oscillations of the breathers vs q.

$$\Phi(x) = A \exp[i(kx - \Delta\mu t)]\mathrm{sech}[A\sqrt{g_3|m_{\mathrm{eff}}|}(x - vt)], \quad (7)$$

with arbitrary amplitude A and wave number k, while the velocity (in fact, the spatial tilt, in terms of planar waveguides) and frequency shift are given by

$$v = k/m_{\mathrm{eff}}, \quad \Delta\mu = (1/2)(g_3A^2 + m_{\mathrm{eff}}v^2), \quad (8)$$

then, the total soliton's frequency is $\mu=\mu_0+\Delta\mu$ [see Eq. (3)].

If the dissipative parameters are finite but small, the total norm of pulse (7), $N=\int_{-\infty}^{\infty}|\Phi(x)|^2dx$, obeys the balance equation,

$$\frac{dN}{dt} = \frac{4A}{\sqrt{g_3|m_{\mathrm{eff}}|}}\left(-\gamma_1 + \frac{2}{3}\gamma_3 g_3 A^2 - \frac{8}{15}\gamma_5 g_5 A^4\right), \quad (9)$$

which can be easily derived from Eq. (1). Condition $dN/dt=0$ predicts the amplitude of a stationary dissipative soliton that may be stable [8].

$$A^2 = \frac{15}{8g_5\gamma_5}\left[\frac{1}{3}\gamma_3 g_1 + \sqrt{\frac{1}{9}(\gamma_3 g_3)^2 - \frac{8}{15}g_5\gamma_1\gamma_5}\right]. \quad (10)$$

[Another fixed point of Eq. (9) is given by expression (10) with the negative sign in front of the radical, but the respective stationary soliton is always unstable [8]]. Solution (10) exists under the condition that the expression under the square root is positive, i.e., the gain is strong enough to compensate the loss.

$$\gamma_3 \geq (\gamma_3)_{\mathrm{min}} \equiv 2\sqrt{(6/5)g_5\gamma_1\gamma_5}/g_3. \quad (11)$$

2. Dark solitons at the center of the Brillouin zone: Analytical and numerical results

In the case of $m_{\mathrm{eff}}>0$ and $\gamma_1=\gamma_3=\gamma_5=0$, Eq. (5) gives rise to the dark-soliton solution,

$$\Phi(x) = A \exp[i(kx - \Delta\mu t)]\tanh[A\sqrt{g_3 m_{\mathrm{eff}}}(x - vt)], \quad (12)$$

$$v = k/m_{\mathrm{eff}}, \quad \Delta\mu = g_3A^2 + (1/2)m_{\mathrm{eff}}v^2, \quad (13)$$

again with arbitrary wave number k and amplitude A (in this case, A is the amplitude of the background that supports the dark soliton). Assuming that small dissipative terms are present, the amplitude of the stable state corresponds to the following fixed point of the norm-balance equation written for the uniform background (far from the center of the dark soliton):

$$A^2 = \frac{g_3\gamma_3 + \sqrt{(g_3\gamma_3)^2 - 4g_5\gamma_1\gamma_5}}{2g_5\gamma_5}, \quad (14)$$

cf. Eq. (10). Obviously, this solution exists under condition [cf. Eq. (11)]

$$\gamma_3 \geq (\gamma_3)_{\mathrm{min}}^{(\mathrm{backgr})} \equiv 2\sqrt{g_5\gamma_1\gamma_5}/g_3. \quad (15)$$

Close to the BZ center, i.e., at small k, the Bloch function may be reasonably approximated (for $\gamma_1=0$) by a combination of three harmonics (see, e.g., Ref. [17]) as follows:

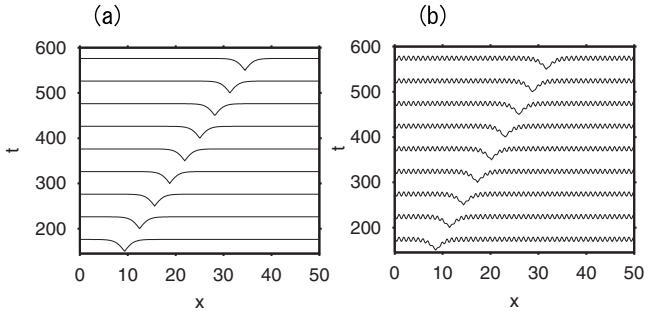

FIG. 3. The evolution of dissipative dark solitons for (a) $\varepsilon=0$ and (b) $\varepsilon=4$, with initial wave number $k=2\pi/100$. Parameters $\gamma_{1,2,3}$ are taken from Eq. (2).

$$F(x) = c_1 \exp(ikx) + c_2 \exp[i(k + 2\pi)x] + c_3 \exp[i(k - 2\pi)x]. \quad (16)$$

Substitution of this into Eq. (4) yields, in the first approximation, $\mu_0(k)=\mu_0^{(\mathrm{center})}+k^2/(2m_{\mathrm{eff}}^{(\mathrm{center})})$, with

$$\mu_0^{(\mathrm{center})} = \pi^2 - \sqrt{\pi^4 + \varepsilon^2/2}, \quad (17)$$

and the positive effective mass,

$$m_{\mathrm{eff}}^{(\mathrm{center})} = \frac{2\pi^4 + \varepsilon^2 + \pi^2\sqrt{4\pi^4 + 2\varepsilon^2}}{10\pi^4 + \varepsilon^2 - 3\pi^2\sqrt{4\pi^4 + 2\varepsilon^2}}. \quad (18)$$

Other coefficients in Eqs. (16) are found to be $c_1=1, c_2=c_3=-\mu_0^{(\mathrm{center})}/\varepsilon$. Then, it follows from Eq. (6) that the cubic nonlinear coefficient in Eq. (5) is $g_3=(1+12c_2^2+6c_2^4)/(1+2c_2^2)$. Further, Eqs. (3) and (12) yield the following full expression for the dark-soliton solution, obtained in the lowest-order approximation for small k (recall that in this section we fix $q=2$):

$$\phi(x,t) = A \exp[im_{\mathrm{eff}}^{(\mathrm{center})}vx - i(\mu_0^{(\mathrm{center})} + \Delta\mu)t][1 + 2c_2\cos(2\pi x)]\tanh[A\sqrt{g_3 m_{\mathrm{eff}}^{(\mathrm{center})}}(x - vt)], \quad (19)$$

where $\Delta\mu$ is given by Eq. (13).

Figures 3(a) and 3(b) display moving dark solitons, as found from direct simulations of Eq. (1) with $\varepsilon=0$ and 4, respectively, while parameters $\gamma_{1,3,5}$ are fixed as per Eq. (2). In both cases, the initial conditions are set with $k=2\pi/100$. The velocities of the dark solitons are numerically found to be $v\approx0.0628$ for $\varepsilon=0$, and $v\approx0.0579$ for $\varepsilon=4$. According to Eq. (13), the respective values of the effective mass are estimated as 1 and 1.084, for $\varepsilon=0$ and 4, respectively, which is close to the analytical results given by Eq. (18): $m_{\mathrm{eff}}(\varepsilon=0)=1$, $m_{\mathrm{eff}}(\varepsilon=4)=1.082$.

3. Bright and dark solitons near edges of the Brillouin zones

At the BZ edge, i.e., near $k=\pi$, one may approximate the Bloch function by a combination of two harmonics [17] as follows:

$$F(x) = c_1 \exp(ikx) + c_2 \exp[i(k - 2\pi)x]. \quad (20)$$

The substitution of this into Eq. (4) yields $\mu_0(k)=\mu_0^{(\mathrm{edge})}+(k-\pi)^2/(2m_{\mathrm{eff}}^{(\mathrm{edge})})$, where

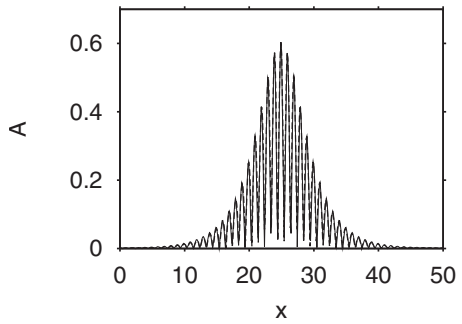

FIG. 4. Comparison of a numerically obtained dissipative gap soliton (solid curve) with the analytical approximation as described in the text (dashed curve), at parameter values taken from Eq. (2). In fact, the solid and dashed lines almost competely overlap.

$$\mu_0^{(\mathrm{edge})} = \frac{1}{2}(\pi^2 \pm |\varepsilon|)2, \quad m_{\mathrm{eff}}^{(\mathrm{edge})} = \frac{|\varepsilon|}{|\varepsilon| \pm 2\pi^2}, \qquad (21)$$

and Eq. (6) yields $g_3=3/4$. The signs + and − in Eq. (21) correspond to the second and first Bloch bands, respectively. It is seen from here that the effective mass (21) for the linear excitations near the BZ edge is *negative* in the first Bloch band for $|\varepsilon|<2\pi^2$ (the latter condition holds in physically relevant situations), while in the second Bloch band the effective mass is positive. These two possibilities suggest the existence of respective bright and dark solitons.

In the former case, the full expression for the bright soliton carried by the Bloch wave near the BZ edge in the first Bloch band is given by Eqs. (3), (7), and (20):

$$\phi(x) = A \exp[im_{\mathrm{eff}}^{(\mathrm{edge})} vx - i(\mu_0^{(\mathrm{edge})} + \Delta\mu)t] \times \cos(\pi x)\mathrm{sech}[A\sqrt{g_3|m_{\mathrm{eff}}^{(\mathrm{edge})}|}(x - vt)]. \qquad (22)$$

Figure 4 compares a typical example of a numerically obtained DGS with its analytical counterpart predicted by Eq. (22) (the dashed curve).

It is worthy to note that, for parameters taken as per Eq. (2), the soliton's frequency shift given by Eq. (8) with $v=0$ is $\Delta\mu=(1/2)g_3A^2\approx 0.13$, where g_3 and A^2 were calculated analytically according to Eqs. (6) and (10). On the other hand, since all the solitons in Fig. 1(b) are situated very close to the upper edge of the first Bloch band, $\Delta\mu$ should be very close to (slightly larger than) the width of the band. Indeed, at point $q=2$, for which the above analysis was developed, the numerically found width of the Bloch band is ≈ 0.13, in agreement with this expectation.

Results produced by the systematic numerical analysis are summarized in Fig. 5, where panel (a) displays a region in parameter plane $(\gamma_1/\gamma_3, \varepsilon)$, where the DGS is stable for $\gamma_3=0.2$ and $\gamma_5=0.6$; cf. Eq. (2) (the stability was identified in a straightforward manner, by monitoring the evolution of perturbed solitons in the course of long simulations). Further, Fig. 3(b) displays the soliton's amplitude A as a function of γ_1/γ_3 for $\varepsilon=5$, $\gamma_3=0.2$, and $\gamma_5=0.6$, and compares it with the analytical prediction given by Eq. (10). Evidently, the prediction is very accurate. The amplitude jumps to zero near $\gamma_1/\gamma_3=0.062$, as predicted by Eq. (11).

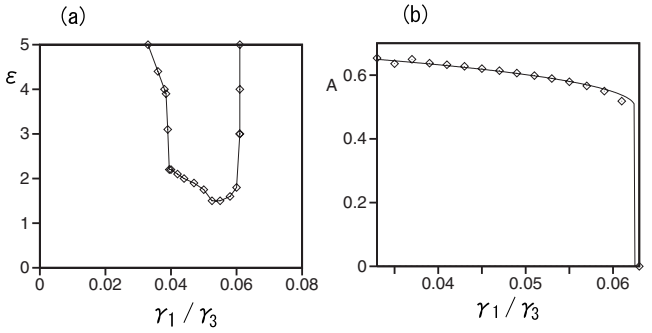

FIG. 5. (a) The numerically identified stability region for the dissipative gap solitons is located above the border, which is shown for $\gamma_3=0.2$, $\gamma_5=0.6$. (b) The amplitude of the dissipative gap solitons vs the inverse gain parameter γ_1/γ_3, for $\varepsilon=5$, $\gamma_3=0.2$, and $\gamma_5=0.6$. The solid line shows the analytical prediction given by Eq. (10) (see the text).

Simulations readily generate moving DGSs too. Figure 6(a) displays an example for $k=2\pi/25$, while the other parameters are fixed as per Eq. (2). In this example, the velocity (actually, the tilt of the spatial soliton) is negative due to the negative effective mass, which is numerically estimated to be ≈ -0.35, as per Eq. (8). The prediction for the same mass, as given by Eq. (21), is −0.34, which is very close to the numerical value. Further, Fig. 6(b) displays a head-on collision of two DGSs with $k=\pm 0.064\pi$. Note that the collision results in an increase of the solitons' velocities. A similar phenomenon was observed in direct simulations of collisions between moving dissipative solitons in the ordinary CQ-CGL equation (without the viscosity, i.e., with no diffusion term), which is tantamount to Eq. (5) [10].

Dark solitons may be carried by the Bloch wave near the BZ edge in the second band, as Eq. (21) yields $m_{\mathrm{eff}}^{(\mathrm{edge})}>0$ in that case. The full form of the approximate solution for the dark soliton follows from Eqs. (3), (7), and (20) [cf. solution (22) for the bright soliton]:

$$\phi(x) = A \exp[im_{\mathrm{eff}}^{(\mathrm{edge})} vx - i(\mu_0^{(\mathrm{edge})} + \Delta\mu)t]\sin(\pi x)\tanh[A\sqrt{g_3 m_{\mathrm{eff}}^{(\mathrm{edge})}}(x - vt)]. \qquad (23)$$

Figure 7(a) displays an example of such a dark soliton for $\varepsilon=7.5$, with the other parameters taken as per Eq. (2). The

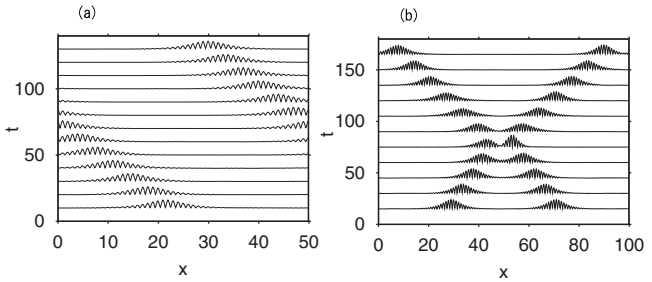

FIG. 6. (a) A stable moving dissipative gap soliton with $k=0.08\pi$, for the parameters chosen as per Eq. (2). (b) The head-on collisions between two solitons in the same case, with $k=\pm 0.064\pi$.

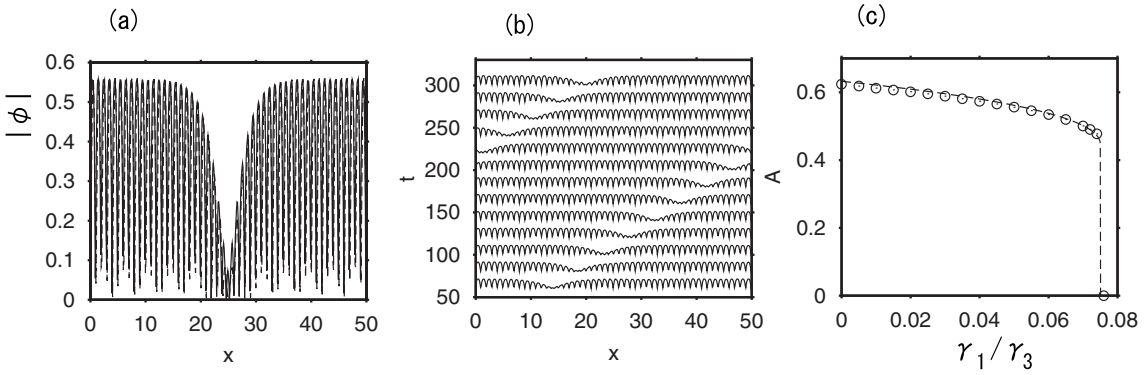

FIG. 7. (a) The numerically generated profile of $|\phi|$ (solid curve) for a dissipative dark soliton, and the analytical approximation given by Eq. (23) and shown by the dashed curve, for $\varepsilon=7.5$, $\gamma_1=0.01$, $\gamma_3=0.2$, and $\gamma_5=0.6$ (the solid and dashed curve merge almost entirely). (b) A moving (tilted) dissipative dark soliton with $k=2\pi/100$, for the same values of the parameters. (c) Amplitude A of the background as a function of γ_1/γ_3 for $\varepsilon=7.5$, $\gamma_3=0.2$, and $\gamma_5=0.6$. The dashed line displays the prediction given by Eq. (14).

comparison shows that Eqs. (23) provides for a good approximation to the shape of the dark soliton, and Eq. (14) accurately approximates the background amplitude [the amplitude drops to zero at $\gamma_1/\gamma_3=0.075$, which exactly corresponds to the critical point predicted by Eq. (15)]. Further analysis of numerical data leads to a conclusion that, for $\gamma_3=0.2$ and $\gamma_5=0.6$, the dark solitons are stable in a relatively narrow interval of values of the strength of the periodic potential, $6.2<\varepsilon<7.8$.

The velocity of the moving dark soliton shown in Fig. 7(b) (in fact, it is the tilt of the beam in the spatial domain, as said above) is numerically evaluated as $v\approx 0.235$. The respective effective mass is evaluated as $k/v\approx 0.267$ [cf. Eqs. (8) and (13)], which is quite close to the analytical prediction 0.275, given for the present case by Eq. (6).

III. DESCRIPTION IN TERMS OF BRAGG SOLITONS

Another approximation for the GSs is relevant in the case when they are found in a narrow band gap. In that case, the field may be represented as a superposition of two waves with propagation constants $\pm\pi q/2$ [in terms of Eq. (1)], which carry slowly varying envelopes $U(x,t)$ or $V(x,t)$ (see, e.g., Ref. [17]).

$$\phi(x,t)=(\sqrt{\varepsilon}/2)[U(x,t)e^{i\pi x}+V(x,t)e^{-i\pi x}] \tag{24}$$

for $q=2$. Substituting this into Eq. (1), keeping only the first derivatives of the slowly varying functions, and defining rescaled variables $\tau\equiv(\varepsilon/2)t$, $\xi\equiv(\varepsilon/2\pi)x$, we arrive at a system of coupled-mode CQ-CGL equations, alias *CGL-Bragg equations*, as follows:

$$\begin{aligned} i\frac{\partial U}{\partial\tau}=&-i\frac{\partial U}{\partial\xi}+\left(\frac{1}{2}|U|^2+|V|^2\right)U-V \\ &+i\left\{-\gamma_1\frac{2}{\varepsilon}+\gamma_3\left(\frac{1}{2}|U|^2+|V|^2\right)\right. \\ &\left.-\gamma_5\frac{\varepsilon}{8}(|U|^4+6|U|^2|V|^2+3|V|^4)\right\}U, \end{aligned}$$

$$\begin{aligned} i\frac{\partial V}{\partial\tau}=&i\frac{\partial V}{\partial\xi}+\left(\frac{1}{2}|V|^2+|U|^2\right)V-U \\ &+i\left\{-\gamma_1\frac{2}{\varepsilon}+\gamma_3\left(\frac{1}{2}|V|^2+|U|^2\right)\right. \\ &\left.-\gamma_5\frac{\varepsilon}{8}(|V|^5+6|U|^2|V|^2+3|U|^4)\right\}V. \end{aligned} \tag{25}$$

In the limit of zero dissipation, $\gamma_{1,3,5}=0$, these equations go over into standard coupled-mode equations derived as a model of the fiber Bragg gratings [15]. The latter equations give rise to a family of well-known analytical solutions in the form of Bragg solitons [14,24] (in fact, it was the first actual example representing the GS species [13]). Those exact solutions can be used as the zero-order approximation, to select the amplitude of the respective DGS from condition $dN/dt=0$ (here, N is the sum of the norms of fields U and V).

We have tested the approximation based on Eqs. (25) by taking numerical solutions of these equations, reconstructing the respective wave forms for ϕ by means of Eq. (24), and comparing them to their counterparts obtained from the simulations of underlying Eq. (1). Figure 8(a) shows a typi-

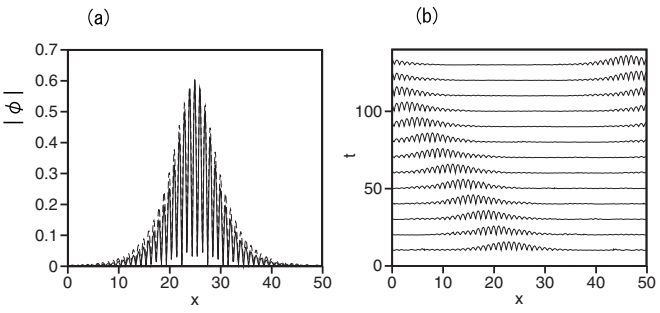

FIG. 8. (a) Comparison of the dissipative gap soliton, obtained in the numerical form from Eq. (1) (solid curve), with the reconstructed profile of $|\phi|$ produced by CGL-Bragg equations (25) (dashed curve), for the parameters chosen as per Eq. (2). (b) An example of the reconstructed profile of $|\phi(x,t)|$ corresponding to a moving dissipative Bragg soliton, at the same set of parameter values.

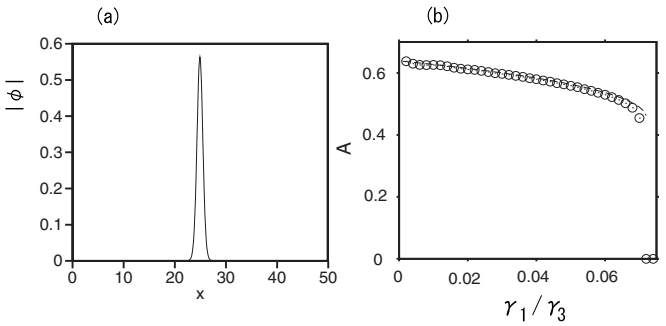

FIG. 9. (a) Profile $|\phi|$ of a typical tightly bound dissipative soliton, obtained as a numerical solution of Eq. (1) for $q=0.5$, with the other parameters fixed as per Eq. (2). (b) Comparison of the numerically found amplitude of the tightly bound solitons with the analytical approximation based on Eqs. (30) (the dashed curve), for $q=1/2$, $\varepsilon=5$, $\gamma_3=0.2$, and $\gamma_5=0.6$.

cal example of the comparison. The amplitude of the dissipative Bragg soliton is slightly larger than its counterpart obtained from the full numerical solution, but the overall agreement is good. DGSs generated by Eqs. (25) can be readily set in motion, as shown in Fig. 8(b).

IV. TIGHTLY LOCALIZED SOLITONS

As wave number πq of the periodic potential decreases, Fig. 1 shows that the dissipative solitons become narrow, and, simultaneously, the Bloch band which separates the first finite band gap from the semi-infinite one turns into a very narrow "shim" between the gaps. A typical example of the narrow (tightly bound) dissipative soliton, found from the numerical solution of Eq. (1), is displayed in Fig. 9(a). The soliton is completely trapped within a single cell of the periodic potential. In contrast to the loosely bound DGSs considered above, tightly bound solitons cannot be set in motion in the simulations.

The shape of the dissipative soliton in Fig. 9(a) suggests the Gaussian ansatz as an analytical approximation for this species of the localized state as follows:

$$\phi \equiv u(x)\exp(-i\mu t) = \pi^{-1/4}\sqrt{N/w}\,\exp[-x^2/(2w^2)]\exp(-i\mu t), \tag{26}$$

where N is the soliton's norm, and w is its width. In conservative models, including the periodic potential and various self-repulsive nonlinearities, this simple ansatz provides, within the framework of the variational approximation, a very accurate fit to tightly bound solitons, which are found if the chemical potential (frequency) is not taken too close to edges of the corresponding band gap [25] [in the present situation, the solitons are close to the lower edge of the band gap, but this proximity is balanced by the fact that the underlying Bloch band is very narrow [see Fig. 1(b)]].

To apply the variational approximation at the zero order, i.e., neglecting the dissipative terms, we note that the Lagrangian of the stationary version of Eq. (1) is

$$L = \int_{-\infty}^{\infty}\left[[\mu+\varepsilon\cos(\pi q x)]u^2 - \frac{1}{2}\left(\frac{du}{dx}\right)^2 - \frac{1}{2}u^4\right]dx. \tag{27}$$

The substitution of ansatz (26) and integration yield the effective Lagrangian,

$$L(N,w) = \mu N - \frac{N}{4w^2} + \epsilon N e^{-q^2\pi^2w^2/4} - \frac{1}{2^{3/2}\sqrt{\pi}}\frac{N^2}{W}. \tag{28}$$

Next, variational equations $\partial L/\partial w = \partial L/\partial N = 0$ give rise to relations

$$N = \frac{\sqrt{2\pi}}{w}[\varepsilon(\pi q)^2 w^4 e^{-(\pi q w/2)^2} - 1], \tag{29}$$

$$\mu = \frac{1}{4w^2} + \frac{N}{\sqrt{2\pi}w} - \varepsilon e^{-(\pi q w/2)^2},$$

which implicitly define a family of the solitons.

Restoring the gain and loss terms with small coefficients $\gamma_{1,3,5}$, we combine Eqs. (29) with the fixed-point condition for the balance equation for the norm [cf. Eq. (9)]. After straightforward manipulations, the following system of equations for N and w can be derived:

$$N = \frac{\sqrt{3\pi}}{2\sqrt{2}}\frac{w}{\gamma_5}\left(\gamma_3 + \sqrt{\gamma_3^2 - \frac{8}{\sqrt{3}}\gamma_1\gamma_5}\right),$$

$$\frac{\varepsilon(\pi q)^2 w^4 e^{-(\pi q w/2)^2} - 1}{w^2} = \frac{\sqrt{3}}{4}\frac{\gamma_3 + \sqrt{\gamma_3^2 - (8/\sqrt{3})\gamma_1\gamma_5}}{\gamma_5}. \tag{30}$$

Figures 1(b) (the dashed line in it) and 9(b) demonstrate very good agreement between the soliton's frequency and amplitude, as predicted by this approximation, and values found from the numerical solution, as long as q is not too large [in fact, for $q \leq 1.5$, as seen in Fig. 1(b)]. In particular, the sudden disappearance of the numerical solution in Fig. 9(b) at $\gamma_1/\gamma_3 \approx 0.072$ is precisely explained by the fact that Eqs. (30) have physical solutions under condition $\gamma_3^2 \geq (8/\sqrt{3})\gamma_1\gamma_5$ [cf. Eqs. (11) and (15)].

V. CONCLUSION

In this work, we have introduced the model combining basic ingredients of conservative systems, which give rise to GSs (gap solitons), i.e., an effective periodic (lattice) potential and self-defocusing cubic nonlinearity, and the set of the loss and gain terms that are basic elements of the CGL equations of the CQ (cubic-quintic type). The model represents the simplest setting in which one may expect the existence of DGSs (dissipative gap solitons), including the more special case of dissipative Bragg solitons, as shown above. The model can be directly realized in terms of spatial optical solitons in planar waveguides with the transverse modulation of the refractive index, self-defocusing nonlinearity, linear gain, and saturable absorption—the ingredients that may be readily found in laser cavities.

Using a combination of direct simulations and several analytical approximations, we have constructed a generic family of stable dissipative solitons. They all belong to the first finite band gap (in terms of the linear spectrum induced by the periodic potential), sitting very close to the border of the Bloch band, which separates the finite band gap from the semi-infinite gap. The soliton family splits into three parts. One subfamily represents loosely bound DGSs, found in the case when the band between the finite and semi-infinite gaps is relatively broad, while the other subfamily contains tightly bound solitons, in the opposite case of a very narrow Bloch band. In fact, the soliton of the latter type is trapped in a single local well of the periodic potential. These two subfamilies are separated by an intermediate one, which consists of stable breathers. The loosely bound DGSs can be accurately described in the framework of two analytical approaches, viz., the product of the Bloch function and slowly varying soliton envelope, and the coupled-mode approximation, which gives rise to a system of *CGL-Bragg equations*. In either case, the approximation is combined with the balance equation for the soliton's norm, to predict the fixed point corresponding to stationary solitons. The former approximation also predicts dissipative dark solitons in the same model. On the other hand, the tightly bound solitons are very accurately described by means of the method combining the variational approximation (based on the Gaussian ansatz) and the fixed point of the balance equation for the norm.

Because the model does not contain the diffusion (viscosity) term, it admits free motion of the loosely bound DGSs (as well as the motion of dark solitons), while the tightly bound solitons, which are firmly pinned to the underlying lattice potential, are immobile. The velocity of the free motion is very accurately predicted by the analytical approximation based on the Bloch functions, and simulations of collisions between moving solitons demonstrate that they pass through each other quasielastically, featuring an increase of the velocity after the collision.

It may be quite interesting to extend the model proposed in this work. In particular, a straightforward possibility is to study dissipative gap solitons in two dimensions, including gap solitons with embedded vorticity.

[1] I. S. Aranson and L. Kramer, Rev. Mod. Phys. **74**, 99 (2002); *Dissipative Solitons*, edited by N. Akhmediev and A. Ankiewicz (Springer, Berlin, Heidelberg, 2005); B. A. Malomed, in *Encyclopedia of Nonlinear Science*, edited by A. Scott (Routledge, New York, 2005), p. 157.

[2] F. T. Arecchi, S. Boccaletti, and P. Ramazza, Phys. Rep. **318**, 1 (1999); M. Ipsen, L. Kramer, and P. G. Sorensen, *ibid.* **337**, 193 (2000); P. Mandel and M. Tlidi, J. Opt. B: Quantum Semiclassical Opt. **6**, R60 (2004).

[3] P. Kolodner, Phys. Rev. Lett. **66**, 1165 (1991); Phys. Rev. A **43**, 2827 (1991); **44**, 6448 (1991); **44**, 6466 (1991); **43**, 4269 (1991).

[4] M. E. Fermann, A. Galvanauskas, G. Sucha, and D. Harter, Appl. Phys. B **65**, 259 (1997); M. F. S. Ferreira, M. M. V. Facão, and S. C. V. Latas, Fiber Integr. Opt. **19**, 31 (2000); F. O. Ilday and F. W. Wise, J. Opt. Soc. Am. B **19**, 470 (2002); Y. D. Gong, P. Shum, D. Y. Tang, C. Lu, X. Guo, V. Paulose, W. S. Man, and H. Y. Tam, Opt. Laser Technol. **36**, 299 (2004); W. H. Renninger, A. Chong, and F. W. Wise, Phys. Rev. A **77**, 023814 (2008).

[5] J. N. Kutz, SIAM Rev. **48**, 629 (2006).

[6] L. M. Hocking and K. Stewartson, Proc. R. Soc. London, Ser. A **326**, 289 (1972); N. R. Pereira and L. Stenflo, Phys. Fluids **20**, 1733 (1977).

[7] V. I. Petviashvili and A. M. Sergeev, Dokl. Akad. Nauk SSSR **276**, 1380 (1984) [Sov. Phys. Dokl. **29**, 493 (1984)].

[8] B. A. Malomed, Physica D **29**, 155 (1987).

[9] O. Thual and S. Fauve, J. Phys. (Paris) **49**, 1829 (1988); S. Fauve and O. Thual, Phys. Rev. Lett. **64**, 282 (1990); W. van Saarloos and P. C. Hohenberg, *ibid.* **64**, 749 (1990); B. A. Malomed and A. A. Nepomnyashchy, Phys. Rev. A **42**, 6009 (1990); V. Hakim, P. Jakobsen, and Y. Pomeau, Europhys. Lett. **11**, 19 (1990); P. Marcq, H. Chaté, and R. Conte, Physica D **73**, 305 (1994); J. M. Soto-Crespo, N. N. Akhmediev, and V. V. Afanasjev, J. Opt. Soc. Am. B **13**, 1439 (1996); O. Descalzi, M. Argentina and E. Tirapegui, Phys. Rev. E **67**, 015601(R) (2003); F. T. Arecchi, S. Boccaletti, and P. Ramazza, Phys. Rep. **318**, 1 (1999); M. Ipsen, L. Kramer, and P. G. Sorensen, Phys. Rep. **337** 193 (2000).

[10] H. Sakaguchi, Physica D **210**, 138 (2005).

[11] H. Sakaguchi and H. R. Brand, Physica D **117**, 95 (1998).

[12] A. Sigler and B. A. Malomed, Physica D **212**, 305 (2005); A. Sigler, B. A. Malomed, and D. V. Skryabin, Phys. Rev. E **74**, 066604 (2006).

[13] W. Chen and D. L. Mills, Phys. Rev. Lett. **58**, 160 (1987); D. L. Mills and S. E. Trullinger, Phys. Rev. B **36**, 947 (1987).

[14] D. N. Christodoulides and R. I. Joseph, Phys. Rev. Lett. **62**, 1746 (1989); A. B. Aceves and S. Wabnitz, Phys. Lett. A **141**, 37 (1989).

[15] C. M. de Sterke and J. E. Sipe, Prog. Opt. **33**, 203 (1994).

[16] O. Zobay, S. Pötting, P. Meystre, and E. M. Wright, Phys. Rev. A **59**, 643 (1999); F. Kh. Abdullaev, B. B. Baizakov, S. A. Darmanyan, V. V. Konotop, M. Salerno, *ibid.* **64**, 043606 (2001); A. Trombettoni and A. Smerzi, Phys. Rev. Lett. **86**, 2353 (2001); G. L. Alfimov, V. V. Konotop, and M. Salerno, Europhys. Lett. **58**, 7 (2002).

[17] H. Sakaguchi and B. A. Malomed, J. Phys. B **37**, 1443 (2004).

[18] B. B. Baizakov, V. V. Konotop, and M. Salerno, J. Phys. B **35**, 5105 (2002).

[19] P. J. Y. Louis, E. A. Ostrovskaya, C. M. Savage, and Y. S. Kivshar, Phys. Rev. A **67**, 013602 (2003); E. A. Ostrovskaya and Y. S. Kivshar, Opt. Express **12**, 19 (2004); Phys. Rev. Lett. **93**, 160405 (2004); H. Sakaguchi and B. A. Malomed, J. Phys. B **37**, 2225 (2004).

[20] B. J. Eggleton, R. E. Slusher, C. M. de Sterke, P. A. Krug, and J. E. Sipe, Phys. Rev. Lett. **76**, 1627 (1996); B. J. Eggleton, C. M. de Sterke, and R. E. Slusher, J. Opt. Soc. Am. B **16**, 587 (1999); J. T. Mok, C. M. de Sterke, I. C. M. Litter, and B. J. Eggleton, Nat. Phys. **2**, 775 (2006).

[21] B. Eiermann, Th. Anker, M. Albiez, M. Taglieber, P. Treutlein,

K.-P. Marzlin, and M. K. Oberthaler, Phys. Rev. Lett. **92**, 230401 (2004); O. Morsch and M. Oberthaler, Rev. Mod. Phys. **78**, 179 (2006).

[22] I. M. Merhasin, B. V. Gisin, R. Driben, and B. A. Malomed, Phys. Rev. E **71**, 016613 (2005); J. Wang, F. Ye, L. Dong, T. Cai, and Y.-P. Li, Phys. Lett. A **339**, 74 (2005).

[23] F. X. Kärtner and U. Keller, Opt. Lett. **20**, 16 (1995); J. N. Kutz, B. C. Collins, K. Bergman, S. Tsuda, S. Cundiff, W. H. Knox, P. Holmes, and M. Weinstein, J. Opt. Soc. Am. B **14**, 2681 (1997).

[24] Yu. I. Voloshchenko, Yu. N. Ryzhov, and V. E. Sotin, Zh. Tekh. Fiz. **51**, 902 (1981) [Sov. Phys. Tech. Phys. **26**, 541 (1981)].

[25] S. K. Adhikari and B. A. Malomed, Europhys. Lett. **79**, 50003 (2007); Phys. Rev. A **76**, 043626 (2007).